

Maximization of ferromagnetism in LaCoO₃ films by competing symmetry

Sisi Li ^{1,2,3}, Jiesu Wang,¹ Qinghua Zhang,¹ Manuel A. Roldan,⁴ Lin Shan,¹ Qiao Jin,¹ Shuang Chen,^{1,5} Zhenping Wu ³,
Can Wang,^{1,6} Chen Ge,¹ Meng He,¹ Haizhong Guo,⁵ Lin Gu ^{1,6,7}, Kui-juan Jin,^{1,6,7,*} and Er-Jia Guo ^{1,2,†}

¹Beijing National Laboratory for Condensed Matter Physics and Institute of Physics, Chinese Academy of Sciences, Beijing 100190, China

²Center of Materials Science and Optoelectronics Engineering, University of Chinese Academy of Sciences, Beijing 100049, China

³State Key Laboratory of Information Photonics and Optical Communications & Laboratory of Optoelectronics Materials and Devices, School of Science, Beijing University of Posts and Telecommunications, Beijing 100876, China

⁴Eyring Materials Center, Arizona State University, Tempe, Arizona 85287, USA

⁵School of Physical Engineering, Zhengzhou University, Zhengzhou 450001, China

⁶School of Physical Sciences, University of Chinese Academy of Sciences, Beijing 100190, China

⁷Songshan Lake Materials Laboratory, Dongguan, Guangdong 523808, China



(Received 18 September 2019; published 15 November 2019)

Spin state transition in perovskite cobaltite is delicately controlled by the competition between exchange interaction energy and crystal-field energy. The latter is mainly governed by the change of bond length and bonding angle. Previous work has revealed that the electronic configuration associated with spin state transition in LaCoO₃ (LCO) thin films can be effectively modulated by epitaxial strain. However, a systematic study on the spin state transition of Co³⁺ ions in LCO films with different crystallographic symmetry is still missing. Here, keeping the in-plane strain unchanged, we report that the magnetization of LCO films can be manipulated with crystallographic symmetry. The ultrathin LCO layers, constrained by the cubic substrate, have pseudotetragonal structure and small magnetization. Upon increasing the layer thickness, the monoclinic structure dominates the LCO film and maximizes its ferromagnetism. For the LCO films with a thickness beyond 35 unit cells, the symmetry relaxes gradually towards its rhombohedral bulk form, and meanwhile the magnetization reduces. These results highlight the importance of spin-lattice entanglement in a ferroelastic material and provide a concise way to maximize its functionality using symmetry engineering.

DOI: [10.1103/PhysRevMaterials.3.114409](https://doi.org/10.1103/PhysRevMaterials.3.114409)

I. INTRODUCTION

Magnetic insulators have attracted tremendous attention due to their potential applications in the *insulating spintronics* [1–3]. Since there is no mobile charge involved in these materials, the excitation of spin in the localized electrons is the primary origin of spin waves that can be converted into charge current *via* the inverse spin Hall effect [4,5]. This advantage reduces greatly the power dissipation compared with other electronic devices based on conductive metals and semiconductors [6,7]. Complex oxides commonly have large bandgaps and contain transition metal ions, offering a large class of magnetic insulating materials [8]. Lanthanum cobaltite, LaCoO₃ (LCO), is a typical material in this context. Bulk LCO is an insulator and has no long-range magnetic ordering at all temperatures [9–12]. The Co³⁺ ions exhibit an active spin state transition, from a low spin (LS, $t_{2g}^6 e_g^0$, $S = 0$) to an intermediate spin (IS, $t_{2g}^5 e_g^1$, $S = 1$) or a high spin (HS, $t_{2g}^4 e_g^2$, $S = 2$) state, with increasing temperature. Previous work revealed an unexpected ferromagnetism observed in the tensile-strained LCO thin films [13–19]. The mechanism behind this compelling result has been debated heavily for years. Oxygen vacancies were first proposed to be the leading

origin of ferromagnetism in LCO films [16,17], because the Co²⁺ ions would have the HS configuration ($t_{2g}^5 e_g^2$, $S = 3/2$) and could form the long-range ferromagnetic ordering easily. However, recent work revealed that negligible Co²⁺ ions are present in the as-grown LCO films, and instead the epitaxial strain plays a crucial role in the spin state transition of Co³⁺ ions [18,19]. This scenario was further supported by both experiments and first-principles calculations [18–22]. The change of strain will affect the competition between the crystal field energy (Δ_{cf}) and intra-atomic exchange interaction energy (Δ_{ex}) through the structural distortion, i.e., the change of bond length (r_{Co-O}) and bonding angle (β) [20–22]. Under a compressive strain, the LS state Co³⁺ ions dominate the LCO films. In this case, the strain-induced distortions of the oxygen octahedra depopulates the e_g electrons causing electron's spins are disfavor magnetic order, which in turn leads to a reduced magnetization [18–20]. With increasing the tensile strain, the magnetization of LCO films increases as the IS or HS state Co³⁺ ions are promoted. To thoughtfully understand the leading role of structural parameters inducing the ferromagnetism in LCO thin films is important for maximizing the performance of spintronic devices. In the past decade, extensive research had been focused on the epitaxial strain effect on the magnetization of LCO thin films [13–22], however, a systematic study on the spin state transition of Co³⁺ ions in LCO films with different symmetry is still missing.

*Corresponding author: kjjin@iphy.ac.cn

†ejguo@iphy.ac.cn

Here we investigate the evolution of crystallographic symmetry in LCO thin films upon increasing layer thickness while keeping the in-plane strain as a constant. We show that the magnetization of LCO films changes systematically with lattice symmetry. Our results provide a direct evidence of the spin-lattice entanglement in perovskite cobaltite thin films and highlight the importance of lattice symmetry to modulate their functionalities in a single strain state.

II. EXPERIMENTAL RESULTS

LCO thin films with a thickness (t_{LCO}) ranging from 5 to 120 unit cells (u.c.) were grown on (001)-oriented TiO_2 -terminated SrTiO_3 (STO) substrates by pulsed laser deposition (see Experimental Section). The LCO films were subsequently capped with a 10-u.c.-thick STO layer to prevent nonstoichiometry in LCO films due to the formation of oxygen vacancies at the surface [19–22]. X-ray diffraction (XRD) measurements confirmed the epitaxial growth of all layers (see Fig. S1 in Ref. [23]). Distinct thickness fringes around the Bragg peaks demonstrate the high quality of all LCO films. Reciprocal space maps (RSM) of all samples were recorded around the substrate's 103 diffraction peak (see Fig. S2 in Ref. [23]), indicating all LCO films are coherently grown with an identical in-plane tensile strain of $\sim 2.5\%$.

X-ray reflectivity (XRR) measurements were performed to verify the thickness of LCO layers and chemical depth profiles. Figs. 1(a)–1(g) show the XRR data (open circles) and their best fits (solid lines) for all LCO films. The chemical depth profiles were obtained from fitting models using GENX [24], as shown in Figs. 1(h)–1(n). The thicknesses of LCO layers and STO capping layers were determined precisely with an accuracy of 1 u.c. (~ 0.4 nm). From the x-ray scattering length density (xSLD) profiles, we found xSLDs for the ultrathin LCO layers ($t_{\text{LCO}} \leq 10$ u.c.) are uniform with a value of $\sim 5.2 \times 10^{-5} \text{ \AA}^{-2}$, close to that of bulk LCO. For the thick LCO layers ($t_{\text{LCO}} \geq 20$ u.c.), xSLD's profiles are nonuniform. The interfacial LCO layers in proximity to STO have a similar xSLD to that of ultrathin LCO layer, whereas the interior part of LCO films has smaller xSLDs by $\sim 2\%$, in agreement with our recent neutron reflectivity results [22]. The uncertainty of xSLD is much smaller than the differences between that of interior and film bulk. This fact may be a consequence of distorted lattice structure owing to the ferroelastic nature of LCO. The formation of ferroelastic domain walls and grain boundaries in the interior part of LCO films likely reduces the atomic density [22] compared with those of the LCO interfacial layers. The XRR results from LCO films with various thicknesses share a similar characteristic, demonstrating a robust nonuniformity of atomic density within an LCO layer that is subject to proximity to STO.

Microstructure analysis of the LCO thin films was performed by high-resolution scanning transmission electron microscopy (STEM). Figure 2(a) shows the cross-sectional high-angle annular dark-field (HAADF) STEM image of a 35-u.c.-thick LCO film. Spatial-resolved electron energy loss spectroscopy (EELS) elemental maps for La- $M_{4,5}$, Co- $L_{2,3}$, and Ti- $L_{2,3}$ edges indicate that the chemical distribution is uniform within each layer [Fig. 2(c)]. Figure 2(d) shows the EELS line profiles of individual elements, revealing the abrupt

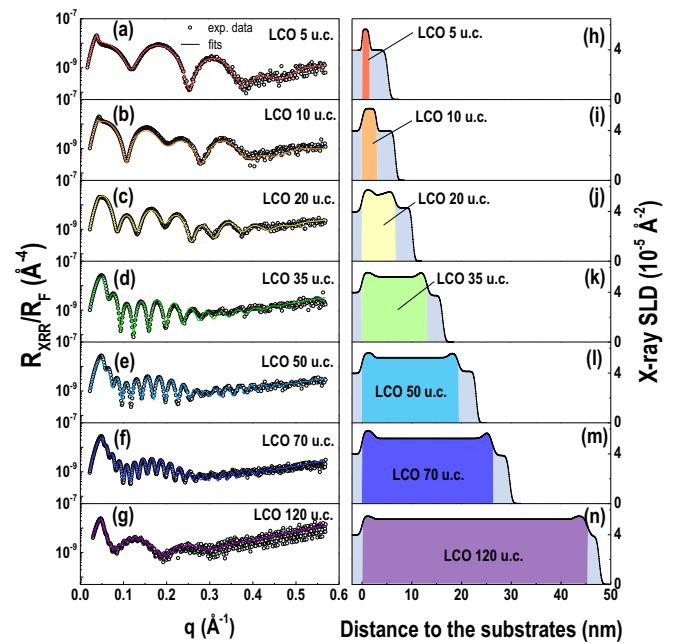


FIG. 1. Determination of LCO layer thickness by x-ray reflectivity (XRR) measurement. [(a)–(g)] XRR curves of LCO films with layer thickness ranging from 5 to 120 u.c., respectively. Open circles are the experimental data and the color lines are the best fits to the XRR data using GENX software. The reflectivity is plotted as a function of the wave-vector transfer $q (=4\pi \sin\theta/\lambda)$ and normalized to the asymptotic value of the Fresnel reflectivity $R_F (=16\pi^2/q^4)$, where θ is the incident angle and λ is the wavelength of x ray. [(h)–(n)] X-ray scattering length density (SLD) depth profiles of LCO films with different layer thickness. All LCO films are capped with 10-u.c.-thick STO layers to prevent the formation of oxygen vacancy at the LCO top surface. XRR fitting results not only provide the accurate layer thickness of STO and LCO, but also indicate the sharp interfaces and smooth surfaces.

interfaces between STO and LCO. The chemical intermixing is limited within 1 u.c. in thickness. The termination is TiO_2 -LaO at both interfaces. Importantly, we observed the well-ordered dark stripes exist only in the interior part of the LCO film with a period of ~ 3 u.c. running perpendicular to the interfaces, consistent with previous reports [18,19]. The interfacial LCO layers close to the STO are free from the dark stripes and have a higher atomic density than that of the interior part. This observation is consistent with our XRR model. To confirm the structural anomaly within an LCO single layer, we measured the cross-sectional HAADF-STEM image of a 10-u.c.-thick LCO film, which has a thickness of the sum of two interfacial layers' width. From Fig. 2(b), no dark stripe is observed within the 10-u.c.-thick LCO layer. These results confirm there is a critical thickness of ~ 5 u.c. for a structural transition within an LCO layer in proximity to STO.

Bulk LCO has a rhombohedral structure, while STO is cubic. The coherent growth of the LCO thin films on STO substrates will inevitably enforce the interfacial LCO layers to be constrained to a high-order symmetry, i.e., pseudotetragonal. Note that both XRR and STEM results illustrate that the atomic densities and interfacial thicknesses at the top and

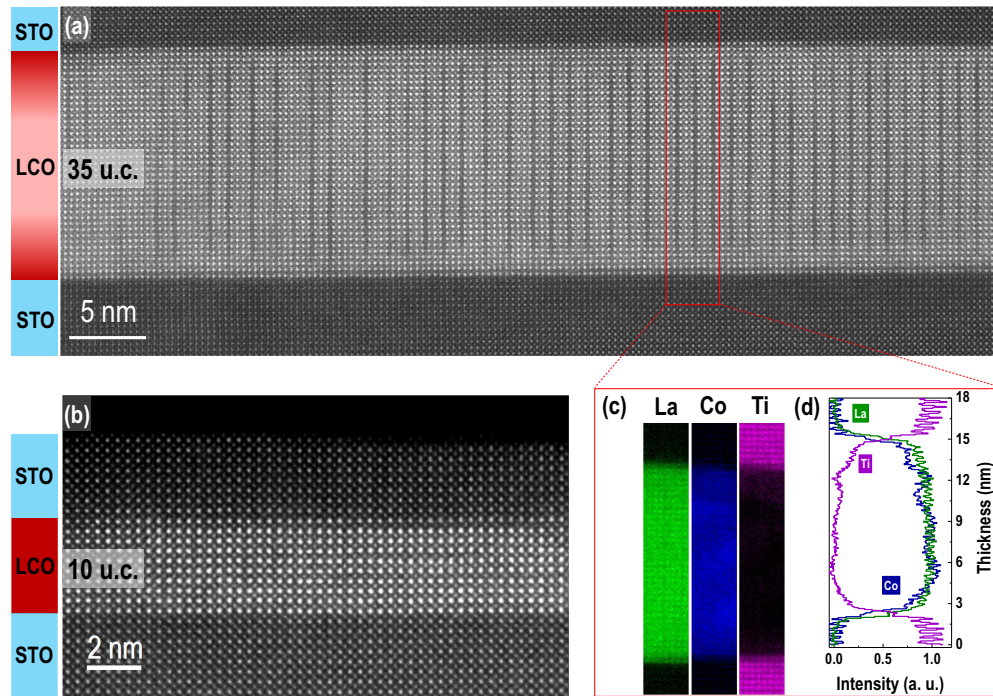


FIG. 2. Microstructure characterization of LCO films. [(a) and (b)] Cross-sectional HAADF-STEM images of 35 u.c.-thick LCO films, respectively. The interface between STO and LCO is continuous and atomically sharp. (c) The colored panels show the integrated intensities of La- $M_{4,5}$, Co- $L_{2,3}$, and Ti- $L_{2,3}$ edges from an area (red square) indicated in (a). (d) Elemental profiles obtained from the EELS line scans across two interface regions, illustrating the distribution of elements within each layer is uniform and the termination at interface is TiO_2 -LaO.

bottom interfaces between LCO and STO are nearly identical, suggesting the structural transition in the LCO layers is dominated by the symmetry mismatch, rather than the misfit strain relaxation. The unusual strain relaxation in the LCO thin films is due to its ferroelastic nature [25,26]. The strain order parameter is strongly coupled to the local stress. Besides the biaxial misfit strain induced by the lattice mismatch, shear strain is present simultaneously between layers with dissimilar crystallographic symmetry. Relaxation of shear strain normally forms nanoscale ferroelastic domains by spontaneous lowering the symmetry while keeping the in-plane strain of LCO films unchanged [27]. Previous work has reported the formation of ferroelastic monoclinic domains in LCO single-crystal and thin films [25–28]. Our work further demonstrates clearly that the thickness for shear strain relaxation (~ 5 u.c.) is much smaller than that for misfit strain relaxation (tens of nanometers) in LCO films. Please note that the dark stripes observed in our work are not caused by ordered oxygen vacancies. Previous works on the as-grown samples indicate the stoichiometry of LCO films with Co^{3+} ions [22,28]. We attribute the dark strips to the ordered monoclinic distorted structure due to the relaxation of shear strain, agreeing with earlier works [18,19].

To corroborate the crystallographic symmetry change in the LCO films, we carried out room-temperature optical second harmonic generation (SHG) measurements in the reflection mode, as shown in Fig. 3(a). Systematic polarimetry measurements on the LCO films with different thicknesses were performed by measuring p - and s -polarized SHG signals, $I_{p\text{-out}}^{2\omega}$ and $I_{s\text{-out}}^{2\omega}$, respectively, while rotating the polarization

(φ) of incident light. Figure 3(b) shows a typical SHG signal from a 10-u.c.-thick LCO film. Solid lines are the best fit to the experimental data (open circles). Optical SHG polarimetry of all LCO films were summarized in Fig. S3 of Ref. [23]. We find that the best fit to the data from LCO ultrathin layers ($t_{\text{LCO}} < 20$ u.c.) is given by the $P4mm$ point group symmetry, whereas the SHG data from the thick LCO layers ($t_{\text{LCO}} > 20$ u.c.) are fitted to the m point group symmetry. In addition, we performed polarimetry measurement on a bare STO substrate (see Fig. S4 in Ref. [23]). The SHG signal from STO is one order of magnitude smaller than those of the LCO films. Therefore the subtle influence from an ultrathin STO capping layer to the SHG signals can be ignored. Figure 3(c) shows the thickness dependent p -polarized SHG signal when a p -polarized light is incident on the LCO films. Solid line describes the trend of the SHG signal as a function of the LCO thickness. It is clear that the SHG signal reduces significantly when $t_{\text{LCO}} \leq 10$ u.c.. With increasing LCO layer thickness, the SHG signal recovers gradually. The optical SHG measurements confirm that the symmetry of LCO films transits from pseudotetragonal ($P4mm$) to monoclinic (m) upon increasing layer thickness.

The intriguing structure transition in the strained LCO films has a strong influence on the magnetization (M) of the LCO films. Magnetization measurements were performed on all LCO films under in-plane magnetic fields. Figure 4(a) shows the temperature (T) dependent magnetization of the LCO films with various thicknesses. $M(T)$ curves exhibit sharp magnetic phase transitions at the Curie temperature (T_C). The inset of Fig. 4(a) summarizes T_C of all LCO films.

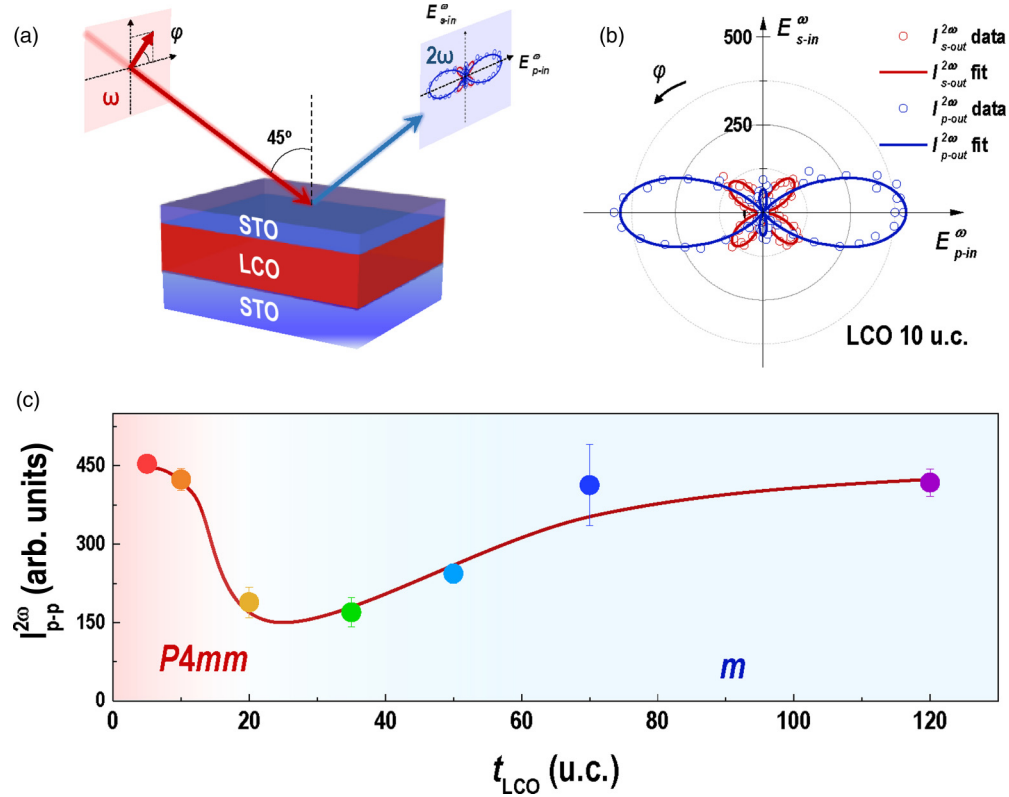


FIG. 3. Optical second harmonic generation (SHG) polarimetry of LCO films. (a) Schematic diagram of SHG measurements carried out in the reflection mode. The incident angle is set to 45° with respect to the sample's surface normal. (b) The polarization (φ) angle dependence of SHG signal from a 10-u.c.-thick LCO film. Two SHG components are plotted, $I_{s\text{-out}}^{2\omega}$ (red) and $I_{p\text{-out}}^{2\omega}$ (blue), with analyzers perpendicular (s -out) and parallel (p -out) to the incidence plane, respectively. Solid lines are the best fits to the SHG data from a 10 u.c.-thick LCO film to the point group symmetry $P4mm$. (c) The SHG signal, $I_{p\text{-p}}^{2\omega}$, as a function of LCO layer thickness (t_{LCO}). We recorded the intensity of reflected p -polarized light after an p -polarized light incidents on the sample. For $t_{\text{LCO}} < 20$ u.c., the SHG data can be fitted to the point group symmetry $P4mm$, whereas the SHG data from thicker LCO films ($t_{\text{LCO}} > 20$ u.c.) are best-fitted to the point group symmetry m .

For $t_{\text{LCO}} \geq 20$ u.c., T_C keeps nearly constant at ~ 80 K, consistent with earlier work [13–15, 18–22]. T_C greatly reduces for the LCO ultrathin layers ($t_{\text{LCO}} \leq 10$ u.c.). Figure 4(b) shows the field (H) dependent magnetization of the LCO films. Except for the 5-u.c.-thick LCO film, all LCO films exhibit clear squarelike hysteresis loops, indicating the ferromagnetic order in the LCO films. The coercivities of all LCO films are nearly the same of ~ 2.5 kOe. We note that the magnetization of the LCO films ($t_{\text{LCO}} \leq 20$ u.c.) does not saturate when H is above 7 T. The continuous increase of magnetization with increasing the magnetic field suggests the paramagnetic component in the LCO films [12], possibly originating from the interfacial LCO layers. With increasing t_{LCO} , the ferromagnetic moment dominates the macroscopic magnetization because the portion of interfacial LCO layers reduces. These observations are consistent with our magnetization depth profiles probed by polarized neutron reflectometry [22]. We show that the magnetic moment of LCO interfacial layers close to the STO is lower than that far from the STO capping/substrates. We attributed this to the tetragonal-monoclinic structural transition upon increasing the LCO layer thickness. Figure 4(c) shows the magnetization of LCO films at 7 T as a function of layer thickness. The magnetization increases abruptly when $t_{\text{LCO}} \leq 20$ u.c. and reaches the maximum value of $1.55 \mu_B/\text{Co}$

for an LCO film with a thickness of 35 u.c. With further increasing t_{LCO} , the magnetization of LCO films decreases gradually.

III. DISCUSSIONS

The nonlinear behavior of thickness dependent magnetization is attributed to the structural transition in LCO films, which affects the spin state of Co^{3+} ion directly via the subtle change in the bonding angle and bond length. In the octahedrally coordinated Co^{3+} , the Co-O molecular orbitals split into threefold degenerate nonbonding t_{2g} levels (d_{xy} , d_{yz} , and d_{xz}) and twofold degenerate antibonding e_g levels ($d_{x^2-y^2}$ and $d_{3z^2-r^2}$), as indicated in Fig. 4(d) [17]. The energy required to excite an electron from t_{2g} to e_g for the spin state crossover is defined as $\Delta = \Delta_{\text{cf}} - \Delta_{\text{ex}} - W$, where $\Delta_{\text{cf}} \propto r_{\text{Co-O}}^{-5}$, $W \propto r_{\text{Co-O}}^{-3.5} \cos(\pi - \beta)$ is the e_g band width, and Δ_{ex} is an intrinsic constant for LCO [29,30]. In the tensile-strained LCO films, the occupation of d electrons in $d_{x^2-y^2}$ orbital is larger compared to $d_{3z^2-r^2}$ orbital due to the lower energy cost [20]. For the LCO films coherently grown on STO, the in-plane lattice constant of LCO ($a_{\text{LCO}} = 3.905 \text{ \AA}$) is larger than twice the $r_{\text{Co-O}}$ in bulk LCO ($r_{\text{Co-O}} = 1.93 \text{ \AA}$). The $r_{\text{Co-O}}$ in our LCO films is larger than that of bulk LCO, leading to a

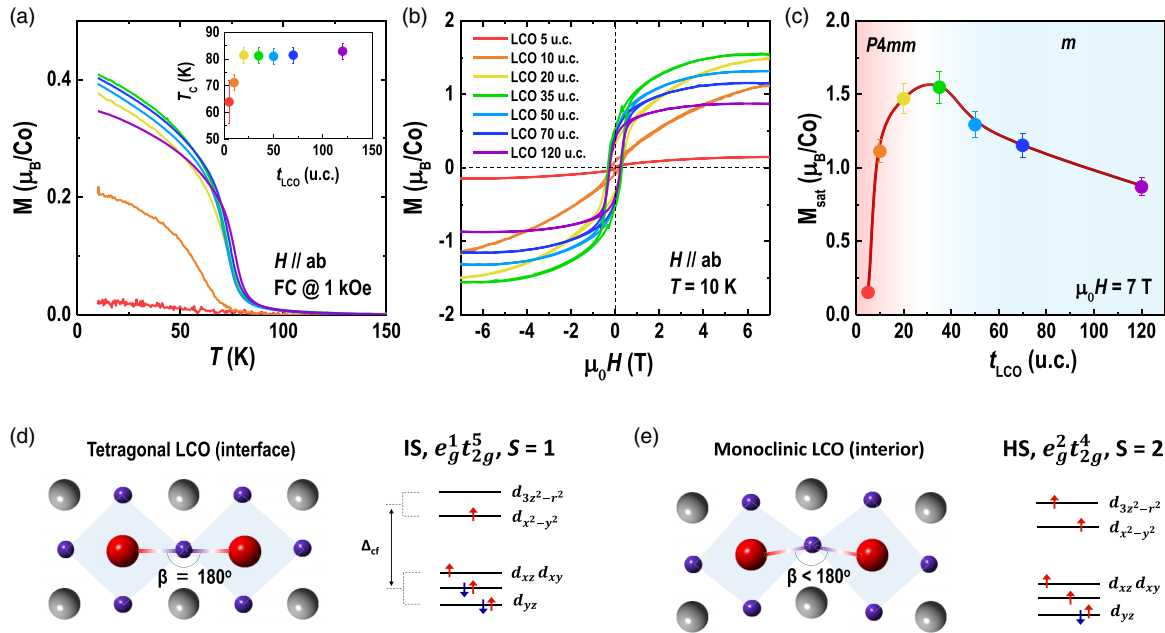


FIG. 4. Magnetic property of LCO films. (a) $M(T)$ and (b) $M(H)$ curves from LCO films with layer thickness ranging from 5 to 120 u.c., respectively. Both measurements were performed under in-plane magnetic fields. $M(T)$ curves were recorded during sample warming after a field cooling of 1 kOe. $M(H)$ curves were measured at 10 K. (c) Magnetic moments at $\mu_0 H = 7$ T were plotted as a function of LCO layer thickness. (d) and (e) Schematics of tetragonal and monoclinic crystal structure, respectively. The electron energy diagram for t_{2g} and e_g orbitals to illustrate the dependence of dominating spin states on the crystallographic symmetry.

decrease of Δ_{cf} , promoting the spin state transition from a LS state to a higher spin state.

The interfacial LCO layers, constrained by STO cubic symmetry, have a pseudotetragonal lattice structure [Fig. 4(d)]. The bonding angle β is close to 180° , and W reaches a maximum value. The bonding angle of ultrathin LCO films is directly calculated by performing the annular bright field (ABF) imaging (see Fig. S5 in Ref. [23]). In this case, the Co^{3+} ions excite from LS into a higher spin state (possibly a mixture of IS and HS). The ultrathin LCO films show the nonzero magnetization. With increasing the layer thickness, the relaxation of shear strain leads the lattice structure of the interior LCO layer transits from a pseudotetragonal ($P4mm$) symmetry to a monoclinic (m) symmetry [Fig. 4(e)]. RSM measurements confirm that all LCO films have the same in-plane lattice constant. XRR and STEM results indicate the atomic density of interior LCO layer is lower than that of the interfacial LCO layer, suggesting a larger averaged octahedral volume, i.e., larger bond length [31], for the interior LCO layer, as a result of reduced bonding angle [18,19]. We estimate the $r_{\text{Co-O}}$ of interior LCO layers increases slightly by $[1 - \cos^{-1}(\frac{180^\circ - \beta}{2})]$ and β decreases from 180° due to the symmetry change. Thus Δ_{cf} reduces, leading to the overall decrease of energy barrier for spin state transition. The population of the HS Co^{3+} ions increases for the monoclinic LCO thin films, exhibiting an increasing magnetization with layer thickness ($10 \text{ u.c.} \leq t_{\text{LCO}} \leq 35 \text{ u.c.}$). This result is consistent with a recent work by Meng *et al.* [21] and Sterbinsky *et al.* [31], suggesting a symmetry-mismatch induced octahedral distortions could effectively increase the population of e_g electrons, leading to the electrons' spins

favor the ferromagnetic order. Furthermore, we also observe a continuous decrease of magnetization for the LCO films when t_{LCO} is beyond 35 u.c. Since the bulk LCO does not have a long-range ferromagnetic ordering, a thicker film should exhibit a similar magnetic ground state as its bulk form. Therefore we attributed the reduction of magnetization in the thick LCO films to the gradual structural relaxation towards the rhombohedral space group symmetry ($R\bar{3}c$ for bulk LCO) [24].

Finally, we note that the termination at the LCO and STO interfaces is $\text{TiO}_2(-1e^-)-\text{LaO}(+1e^-)$, which apparently is charge imbalanced. For the interfaces between polar and nonpolar layers, polar catastrophe commonly forces an interfacial reconstruction via atomic disordering and stoichiometry change at the interface [32,33]. Our STEM and EELS results demonstrate the atomically sharp STO/LCO interfaces with only minor chemical intermixing within 1 u.c. Previously, x-ray absorption spectroscopy (XAS) measurements were conducted at Co L edges in fluorescence yield (FY) mode [20,22]. No signature of Co^{2+} ion is detected, confirming that the oxidation state of Co ions is trivalent in the as-grown LCO films. Therefore the interfacial screening charges have a negligible effect on the overall magnetization of the interfacial LCO layers. Furthermore, we emphasize that the octahedral rotation may play a role in the magnetization enhancement after the crystallographic symmetry changes from tetragonal to monoclinic. The octahedral rotation helps to decrease the hybridization between Co $3d$ and O $2p$ orbitals, thus the magnetic ordering of electron spins is promoted. This argument is supported by both first-principles calculations and experiments, in agreement with our results [29,34,35].

IV. CONCLUSIONS

In conclusion, we report a direct correlation between crystallographic symmetry and macroscopic magnetization in the single strain-state LCO films. Combined with XRD, STEM, and optical SHG measurements, we reveal a systematic variation of structural symmetry in the LCO films with increasing layer thickness. The interfacial LCO layer in proximity to STO, constrained by a high-order symmetry, shows a small magnetization. With increasing the layer thickness, the relaxation of misfit shear strain drives the LCO film into a monoclinic structure, stabilizes the higher spin configuration of the Co^{3+} ions, and enhances the macroscopic magnetization. These results highlight the significance of the lattice symmetry in controlling the spin state transition in the perovskite cobaltite thin films. We believe these observations not only provide new insights in the origin of ferromagnetism in strained LCO films, but also offer an effective pathway to maximize the functionality in magnetic insulators for energy-saving spintronic devices.

ACKNOWLEDGMENTS

We acknowledge fruitful discussions with Dr. H. N. Lee and Dr. M. R. Fitzsimmons at Oak Ridge National Laboratory and Dr. Andreas Herklotz at Martin Luther University Halle-Wittenberg. E.J.G. is supported by the Hundred Talents Program from Chinese Academy of Sciences. M.R. acknowledges the use of facilities within the Eyring Materials Center at Arizona State University. This work was supported by the National Natural Science Foundation of China (Grant No. 11974390), the National Key Basic Research Program of China (Grant No. 2017YFA0303604), the Key Research Program of Frontier Sciences of the Chinese Academy of Sciences (Grant No. QYZDJ-SSW-SLH020), and the Strategic Priority Research Program (B) of the Chinese Academy of Sciences (Grant No. XDB07030200).

The authors declare no competing financial interest.

APPENDIX: EXPERIMENTAL SECTION

1. Thin film growth and basic characterizations

The LCO thin films were fabricated on (001)-oriented STO substrates by pulsed laser deposition. The STO substrates

were pretreated by buffered HF and annealed at high temperature to ensure the TiO_2 terminated surface. The LCO films with different layer thicknesses were grown at a temperature of 700°C and an oxygen partial pressure of 100 mTorr. All LCO films were capped with an ultrathin STO layer with a thickness of 10 u.c. to prevent having a nonstoichiometric surface. XRD and XRR measurements were performed using a Bruker D8 Discovery diffractometer. Magnetization measurements were conducted in a Physical Property Measurement System (PPMS) equipped with a VSM from Quantum Design.

2. STEM and EELS observations

Cross-sectional TEM specimens were prepared by standard focused ion beam lift out techniques and were investigated by a double aberration-corrected 200 kV JEOL ARM equipped with an electron energy loss spectrometer (EELS). The 35-u.c.-thick LCO film was measured at Arizona State University (ASU) and the 10-u.c.-thick LCO film was measured at Institute of Physics, Chinese Academy of Sciences (IOP-CAS). The atomic structures of samples were investigated by high-resolution HAADF imaging. The EELS elemental maps were obtained from a selected area in the HAADF-STEM image. The line profiles from $\text{La-M}_{4,5}$, $\text{Co-L}_{2,3}$, and $\text{Ti-L}_{2,3}$ edges were obtained simultaneously by integrating the intensities from the EELS maps.

3. Optical SHG polarimetry measurements

Optical SHG measurements were performed in the reflection geometry [see Fig. 3(a)] using an 800-nm-wavelength probing laser beam from a Ti: Sapphire femtosecond laser (Tsunami 3941-X1BB, Spectra-Physics). The linear polarized laser beam with a change in the polarization direction (φ) is incident on the sample at an angle of 45° . The reflection SHG signals were decomposed into p - and s -polarized components and detected by a photon multiplier tube. Systematic polarimetry measurements were conducted by scanning polarization of incident beam for all LCO films. All measurements were conducted at room temperature.

-
- [1] K. Uchida, J. Xiao, H. Adachi, J. Ohe, S. Takahashi, J. Ieda, T. Ota, Y. Kajiwara, H. Umezawa, H. Kawai, G. E. W. Bauer, S. Maekawa, and E. Saitoh, *Nat. Mater.* **9**, 894 (2010).
 - [2] S. Y. Huang, X. Fan, D. Qu, Y. P. Chen, W. G. Wang, J. Wu, T. Y. Chen, J. Q. Xiao, and C. L. Chien, *Phys. Rev. Lett.* **109**, 107204 (2012).
 - [3] A. Kehlberger, U. Ritzmann, D. Hinzke, E. J. Guo, J. Cramer, G. Jakob, M. C. Onbasli, D. H. Kim, C. A. Ross, M. B. Jungfleisch, B. Hillebrands, U. Nowak, and M. Kläui, *Phys. Rev. Lett.* **115**, 096602 (2015).
 - [4] J. Xiao, G. E. W. Bauer, K. Uchida, E. Saitoh, and S. Maekawa, *Phys. Rev. B* **81**, 214418 (2010).
 - [5] L. Wang, R. J. H. Wesselink, Y. Liu, Z. Yuan, K. Xia, and P. J. Kelly, *Phys. Rev. Lett.* **116**, 196602 (2016).
 - [6] C. M. Jaworski, J. Yang, S. Mack, D. D. Awschalom, J. P. Heremans, and R. C. Myers, *Nat. Mater.* **9**, 898 (2010).
 - [7] K. Uchida, S. Takahashi, K. Harii, J. Ieda, W. Koshibae, K. Ando, S. Maekawa, and E. Saitoh, *Nature (London)* **455**, 778 (2008).
 - [8] K. J. Jin, H. B. Lu, K. Zhao, C. Ge, M. He, and G. Z. Yang, *Adv. Mater.* **21**, 4636 (2009).
 - [9] P. M. Raccah and J. B. Goodenough, *Phys. Rev.* **155**, 932 (1967).
 - [10] J. -Q. Yan, J. -S. Zhou, and J. B. Goodenough, *Phys. Rev. B* **70**, 014402 (2004).
 - [11] A. Podlesnyak, S. Streule, J. Mesot, M. Medarde, E. Pomjakushina, K. Conder, A. Tanaka, M. W. Haverkort, and D. I. Khomskii, *Phys. Rev. Lett.* **97**, 247208 (2006).

- [12] S. Zhou, L. Shi, J. Zhao, L. He, H. Yang, and S. Zhang, *Phys. Rev. B* **76**, 172407 (2007).
- [13] D. Fuchs, C. Pinta, T. Schwarz, P. Schweiss, P. Nagek, S. Schuppler, R. Scheider, M. Merz, G. Roth, and H. v. Löhneysen, *Phys. Rev. B* **75**, 144402 (2007).
- [14] J. W. Freeland, J. X. Xia, and J. Shi, *Appl. Phys. Lett.* **93**, 212501 (2008).
- [15] A. Herklotz, A. D. Rata, L. Schultz, and K. Dörr, *Phys. Rev. B* **79**, 092409 (2009).
- [16] N. Biškup, J. Salafranca, V. Mehta, M. P. Oxley, Y. Suzuki, S. J. Pennycook, S. T. Pantelides, and M. Varela, *Phys. Rev. Lett.* **112**, 087202 (2014).
- [17] V. V. Mehta, N. Biskup, C. Jenkins, E. Arenholz, M. Varela, and Y. Suzuki, *Phys. Rev. B* **91**, 144418 (2015).
- [18] W. S. Choi, J. -H. Kwon, H. Jeon, J. E. Hamann-Borrero, A. Radi, S. Macke, R. Sutarto, F. He, G. A. Sawatzky, V. Hinkov, M. Kim, and H. N. Lee, *Nano Lett.* **12**, 4966 (2012).
- [19] J.-H. Kwon, W. S. Choi, Y.-K. Kwon, R. Jung, J.-M. Zuo, H. N. Lee, and J. Kim, *Chem. Mater.* **26**, 2496 (2014).
- [20] E. J. Guo, R. D. Desautels, D. Keavney, A. Herklotz, T. Z. Ward, M. R. Fitzsimmons, and H. N. Lee, *Phys. Rev. Mater.* **3**, 014407 (2019).
- [21] D. Meng, H. Guo, Z. Cui, C. Ma, J. Zhao, J. Lu, H. Xu, Z. Wang, X. Hu, Z. Fu, R. Peng, J. Guo, X. Zhai, G. J. Brown, R. Knize, and Y. Lu, *Proc. Natl. Acad. Sci. USA* **115**, 2873 (2018).
- [22] E. J. Guo, R. Desautels, D. Lee, M. A. Roldan, Z. Liao, T. Charlton, H. Ambayer, J. Molaison, R. Boehler, D. Keaveny, A. Herklotz, T. Z. Ward, H. N. Lee, and M. R. Fitzsimmons, *Phys. Rev. Lett.* **122**, 187202 (2019).
- [23] See Supplemental Material at <http://link.aps.org/supplemental/10.1103/PhysRevMaterials.3.114409> for structural and SHG characterizations.
- [24] M. Björck and G. Andersson, *J. Appl. Cryst.* **40**, 1174 (2007).
- [25] P. E. Vullum, R. Holmestad, H. L. Lein, J. Mastin, M.-A. Einarsrud, and T. Grande, *Adv. Mater.* **19**, 4399 (2007).
- [26] E. K. H. Salje and F. Materials, *Annu. Rev. Mater. Res.* **42**, 265 (2012).
- [27] E.-J. Guo, R. Desautels, D. Keavney, M. A. Roldan, B. J. Kirby, D. Lee, Z. Liao, T. Charlton, A. Herklotz, T. Z. Ward, M. R. Fitzsimmons, and H. N. Lee, *Sci. Adv.* **5**, eaav5050 (2019).
- [28] D. Fuchs, E. Arac, C. Pinta, S. Schuppler, R. Schneider, and H. v. Löhneysen, *Phys. Rev. B* **77**, 014434 (2008).
- [29] K. Knizek, P. Novak, and Z. Jirak, *Phys. Rev. B* **71**, 054420 (2005).
- [30] L. Qiao, J. H. Jang, D. J. Singh, Z. Gai, H. Xiao, A. Mehta, R. K. Vasudevan, A. Tselev, Z. Feng, H. Zhou, S. Li, W. Prellier, X. Zu, Z. Liu, A. Borisevich, A. P. Baddorf, and M. D. Biegalski, *Nano Lett.* **15**, 4677 (2015).
- [31] G. E. Sterbinsky, P. J. Ryan, J.-W. Kim, E. Karapetrova, J. X. Ma, J. Shi, and J. C. Woicik, *Phys. Rev. B* **85**, 020403(R) (2012).
- [32] A. Ohtomo, D. A. Muller, J. L. Grazul, and H. Y. Hwang, *Nature (London)* **419**, 378 (2002).
- [33] N. Nakagawa, H. Y. Hwang, and D. A. Muller, *Nat. Mater.* **5**, 204 (2006).
- [34] E. J. Moon, P. V. Balachandran, B. J. Kirby, D. J. Keavney, R. J. Sichel-Tissot, C. M. Schlepütz, E. Karapetrova, X. M. Cheng, J. M. Rondinelli, and S. J. May, *Nano Lett.* **14**, 2509 (2014).
- [35] Z. Liao, M. Huijben, Z. Zhong, N. Gauquelin, S. Macke, R. J. Green, S. Van Aert, J. Verbeeck, G. Van Tendeloo, K. Held, G. A. Sawatzky, G. Koster, and G. Rijnders, *Nat. Mater.* **15**, 425 (2016).